ACS OMEGA

Open Access

http://pubs.acs.org/journal/acsodf

Article

ASSERT: A Platform Technology for Rapid Electrochemical Sensing of Soil Ammonium

Mohammed A Eldeeb, Vikram Narayanan Dhamu, Anirban Paul, Firas Maqsood Alam, E. Natalie Burgos, Sriram Muthukumar, and Shalini Prasad*

Cite This: *ACS Omega* 2024, 9, 33928−33934

Read Online

ACCESS | Metrics & More | Article Recommendations | Supporting Information

ABSTRACT: The world is facing a food shortage predicament largely fueled by inefficient, outdated farming conventions that are passed down from generation to generation. Overfertilization is one of the major byproducts of inadequate farming techniques. This leads to an imbalance in the soil ecosystem, affecting carbon sequestration, plant-available nutrients, and microorganisms. Sustainable agriculture, on the other hand, efficiently uses the soil with minimal fertilizer and crop rotation to prevent soil erosion. This method requires real-time information on the soil's health. An electrochemical ion-selective electrode (ISE) is presented to measure soil ammonium in situ. The sensor utilized electrochemical impedance spectroscopy for direct, continuous soil ammonium measurement without any soil pretreatment. The ISE is applied by drop-casting onto the working electrode. The sensor response was calibrated against the three main different soil textures (clay, sandy loam, and loamy clay) to cover the entirety of the soil texture triangle. The linear regression models showed an ammonium-dependent response with Pearson $r > 0.991$ for the various soil textures in the range of 2−32 ppm. The sensor response was validated against the gold standard spectrophotometric method after KCl extraction showed a less than 20% error rate between the measured ammonium and reference ammonium. A 16 day in situ soil study showed the capability of the sensor to measure soil ammonium in a temporally dynamic manner with a coefficient of variance of 11%, showing robust stability for in situ monitoring.

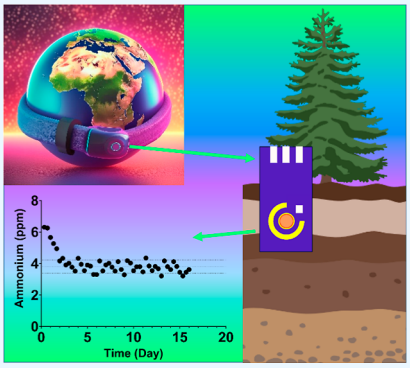

1. INTRODUCTION

Over seven decades ago, the green revolution started incorporating technological advancements in the field of agriculture. More efficient irrigation systems, the use of a cheaper synthetic fertilizer, and large-scale machinery are some of the improvements brought by the green revolution. There was an increase in plant gene editing for higher crop yield, faster plant growth, and enhanced immunity against pests and extreme weather. Coupled together, the green revolution more than doubled the production of some of the world's staple food products like rice, wheat, and corn. Nevertheless, food insecurity is listed in the United Nation's Sustainable Development Goals report as food supply lags the rise in demand.[1] Rising prices due to political conflict, the COVID-19 pandemic, and global warming causing extended droughts have all contributed to the worsening of food security worldwide.[2] As such, multiple organizations are pushing toward sustainable agriculture.[3] The National Institute of Food and Agriculture defines sustainable agriculture as a system that integrates plant and animal production that, over the long-term, would satisfy human food requirements, protect the environment and enhance its natural resources, make efficient use of non-renewable resources supported by the ecological cycle, and improve the quality of life for society and farmers.[3] Sustainable agriculture thus requires farmers to track the health of their soil throughout the year.[4−6] Currently, the standard for measuring soil ammonium is by using a spectrophotometric method after extraction with potassium chloride solution. This method requires days to air-dry the soil sample. Then, the soil is mixed with potassium chloride in a 1:2 (w/v) ratio before measuring the ammonium concentration using a spectrophotometer. Due to the high expenses of soil analysis, farmers tend to test their land once every two to five years. The severity of the food shortage sparked a surge in research on reliable in situ methods for continuous measurement of soil nutrients.[7]

A common technique is image analysis using drone or satellite images.[8−11] Other methods include optical sensors that have good sensitivity; however, they greatly suffer from bulky spectrometer hardware, site-specific calibration, and a lack of accuracy for detecting nutrients that are not fully observed in the visible−near-infrared region.[12,13] Another approach uses a robotic platform that scans a specific field, detecting different vegetation and assessing the irrigation cycle

Received: May 1, 2024
Revised: June 28, 2024
Accepted: July 2, 2024
Published: July 25, 2024

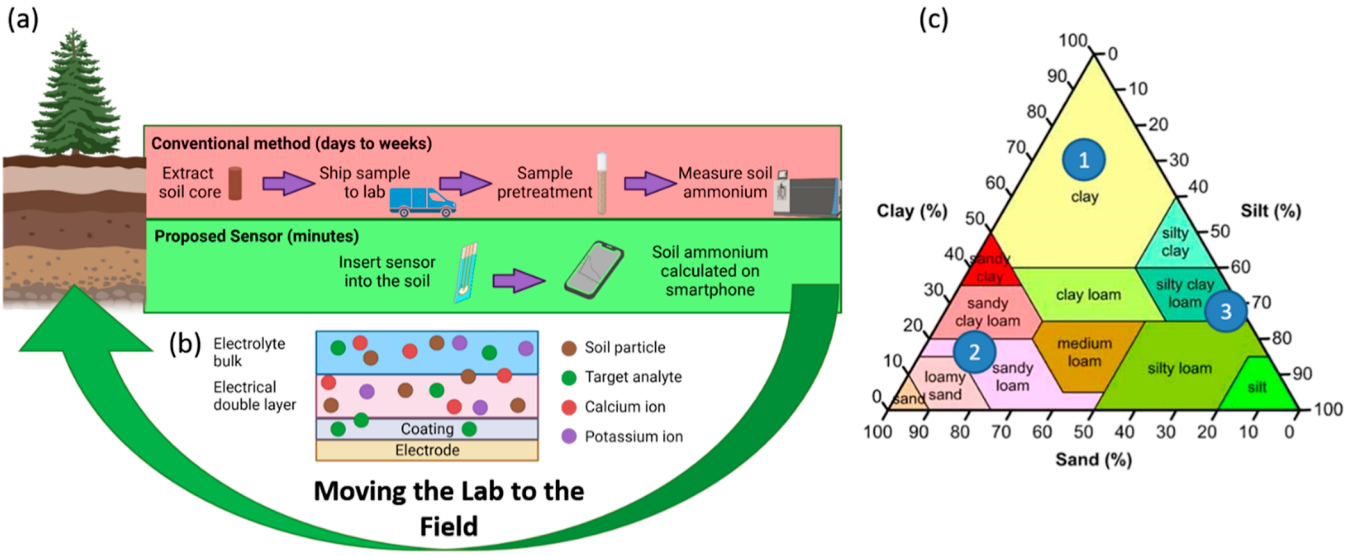

Figure 1. (a) Illustration of the current soil analysis method vs the proposed method of miniaturized sensors for in situ monitoring. (b) Illustration of the EDL formed at the interface between the soil and the electrode surface. The ion-selective coating allows the diffusion or binding of a specific target ion alone, which in this case is ammonium. (c) Soil triangle illustrating the different textures of soil depending on the different ratios of clay, sand, and silt content.

for the different fields.[14] These methods require collecting thousands of images stitched together and large processing power to analyze the data. On the other hand, miniaturized sensors require a microcontroller and a battery in a hand-held device to measure soil nutrients.[15−21] The simplicity of the hardware allows for weeks or months of data collection before the batteries need to be replaced. The sensors are calibrated on the soil samples, ensuring high measurement accuracy in situ. Screen-printed electrodes are the most common type of sensors used for their low cost, portability, and ease of insertion in the soil, as illustrated in Figure 1b. Fayose et al. developed a nonactin-based ammonium ion-selective electrode (ISE) with a limit of quantification of 0.9 ppm in soil extract.[22] Garland et al. also utilized nonactin in a polyvinyl chloride (PVC) membrane on top of laser-induced graphene electrodes to measure ammonium concentration in soil slurries with a limit of quantification of 1.5 ppm.[23] Similarly, multiple research studies were carried out using nonactin-based ISE in either soil or water samples with a detection limit as low as 1 ppm in soil extract.[18,24−26] First, all these studies were conducted using open-circuit potential measurements. Open-circuit potential measures the equilibrium state of soil, which is highly susceptible to environmental noise, signal drift, and moisture content in soil. As such, these sensors are not suitable for long-term in situ measurement. Furthermore, none of the studies conducted a long-term study on the lifetime or reliability of these sensors in situ. This work showcases the first-of-its-kind real-time continuous in situ soil ammonium measurement through the use of electrochemistry. Electrochemical impedance spectroscopy (EIS) captures a more wholesome picture of the electrical double layer (EDL) formed at the interface between the electrode and the soil slurry.[20] As such, the concentration of specific nutrients can be extracted at different frequencies.[27−29] Due to the vast differences in soil textures, the sensor was calibrated in three different soil textures with varying clay, sand, and silt concentrations. The three soil textures are clay, sandy loam, and loamy clay, as indicated on the soil texture triangle in Figure 1c. A 16 day study was followed to showcase the capability of the sensor for continuous in situ monitoring. Finally, this work is the first proof of feasibility in integrating electrochemical sensors in a monitoring system for real-time continuous tracking of the dynamic soil ecosystem.

2. MATERIALS AND METHODS

2.1. Materials. Screen-printed three-electrodes (Dropsens 220AT) with gold working and counter electrodes and a silver reference electrode were bought from Metrohm (Herisau, Switzerland). Ammonium ionophore I, high-molecular-weight poly(vinyl chloride) (PVC), bis(2-ethylhexyl) sebacate (DOS), 1-butyl-3-methylimidazolium bis-(trifluoromethylsulfonyl)imide (BMIM [TF2N]), tetrahydrofuran (THF) stabilized with BHT, and ammonium chloride were bought from Sigma-Aldrich (MA, USA). The portable potentiostat EmStat Pico was purchased from PalmSens (Houten, the Netherlands). Gaussian software Gaussian 16 W, version 1.1 (CT, USA), was used to perform the computational study. All statistical analysis and figure plots were determined using Graphpad Prism, version 10.2.0 (California, US). Illustrative sketches were drawn using BioRender.

2.2. Soil Sample Preparation. Three different soil types were used: clay, loamy clay, and sandy loam. These soil types provide full coverage of the soil texture triangle illustrated in Figure 1c. Air-dried soil was ground and filtered through a 2 mm mesh to acquire fine soil particles. The air-dried soil samples used had an ammonium concentration of less than 1 ppm, which is considered the baseline or 0 ppm sample. Dilutions of ammonium chloride (NH_4Cl) dissolved in deionized (DI) water were prepared to acquire 7 samples with final ammonium concentrations of 0, 2, 4, 8, 16, 24, and 32 ppm. A mixture of 4 mL of soil and 2 mL of the corresponding NH_4Cl solution was prepared for each soil type to acquire soil slurries with 50% water content mimicking agriculture conditions. All soil samples were prepared the day before the experiment began to provide adequate time to ensure that all samples were homogeneous.

https://doi.org/10.1021/acsomega.4c04181
ACS Omega 2024, 9, 33928−33934

2.3. Electrode Preparation. To prepare the ammonium-selective coating, 35 mg of PVC and 65 mL of DOS were dissolved in 1000 μL of THF, as illustrated in Figure 2a. The

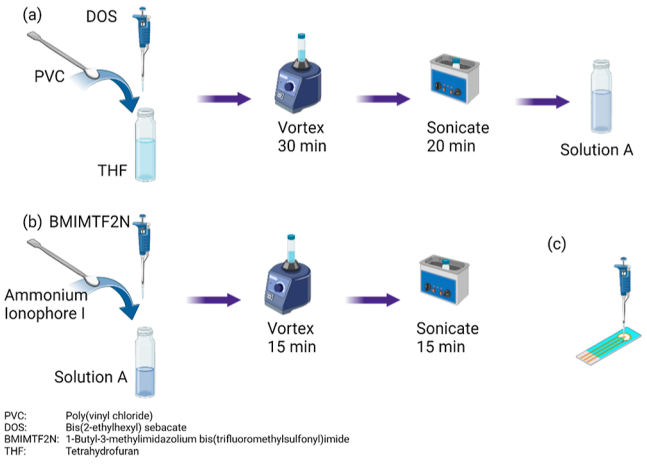

Figure 2. (a) Ammonium ion-selective coating fabricated by mixing PVC powder and the DOS plasticizer in THF and then stirring and sonicating until a clear homogeneous solution is obtained. (b) Then, the RTIL BMIM [TF2N] and ammonium ionophore I are dissolved in the solution previously prepared by mechanically stirring and placing in a sonic bath until a clear homogeneous solution is obtained. (c) Finally, drop-casting of the ion-selective coating onto the working electrode.

solution was mechanically stirred for 30 min, followed by 20 min of sonication in a water bath. Afterward, 5 mg of ammonium ionophore I and 1 μL of BMIM [TF2N] were added in a new glass vial with 194 μL from the solution previously prepared, solution A. The new solution was mechanically stirred for 15 min, followed by sonication in a water bath for 15 min. Finally, 2 μL of the solution was drop-casted onto the working electrode and left overnight to dry at room temperature, as shown in Figure 2c.

2.4. Experimental Design. A printed circuit board was designed to host the potentiostat, EmStat Pico, and provide connectivity to a computer through a USB cable with a connector to plug in the sensor. All measurements were conducted through the PSTrace software provided by PalmSens. The prepared soil samples were incubated on the sensors for 5 min before the measurement was taken. EIS was run from 100 kHz to 100 Hz with an amplitude of 15 m V_{RMS} and 0 V DC bias.

3. RESULTS AND DISCUSSION

3.1. Simulation. By evaluating the interaction of several room-temperature ionic liquids (RTILs) with an ammonia molecule, the free energy and enthalpy have been recorded accordingly and are summarized in Table 1. The goal is to choose a RTIL which shows lower free energy and depicts the spontaneity of the interaction; hence, it proved to be the best transducer for this application. A total of six numbers of RTILs have been simulated with an ammonia molecule using the standard Gaussian software and Hartree−Fock method, with a basis set of 6-31g (d). The simulations have been performed by putting the RTIL and the ammonia molecule in close vicinity, and the thermodynamic properties of RTIL−ammonia interactions have been duly tabulated and are presented in Table 1.

Table 1. RTIL−Ammonia Interaction Result

RTIL	EE + free energy (hartree)	EE + enthalpy (hartree)
ammonia	+0.004876	+0.026658
BMIM [Cl]-NH_3	+0.341452	+0.407709
BMIM [BF_4]-NH_3	−894.346	−894.275
EMIM [BF_4]-NH_3	−816.762	−816.700
EMIM [TF_2N]-NH_3	−2207.581	−2207.492
BMIM [TF_2N]-NH_3	−2285.163	−2285.067

The result shows a consecutive decrement of Gibbs free energy of ammonia upon the introduction of RTILs. These five RTILs were chosen due to their superior conductivity, viscosity, and electrochemical properties, which make them widely utilized for electrochemical sensing applications. Based on the RTIL−ammonia simulation result, the Gibbs free energy and enthalpy of the MIM [TF_2N]-based RTIL are much lower than those of other MIM-based RTILs. Similarly, BMIM [TF_2N] has lower Gibbs free energy and enthalpy compared to those of its EMIM analogue, suggesting the selection of BMIM [TF_2N] for actual electrochemical application purposes.[28]

Then, BMIM [TF_2N] has been utilized to understand the interaction of the RTIL with the ammonium ion. The simulation has been subdivided into three sections to better understand the interaction. The simulation has been performed using Gaussian software with the Hartree−Fock method, with a basis set of 631-G (d). The result is depicted in Figure 3, where Figure 3a depicts the optimized structure of pristine BMIM [TF_2N], where a clear noncovalent interaction has been observed between the N of the imidazole ring of $BMIM^+$ and the N of the bistriflimide (TF_2N^-) fragment, suggesting the stability of the RTIL, which stays in a zwitterionic architecture. Furthermore, the RTIL has been simulated with the NH_4^+ ion by putting it in close proximity, and the result is depicted in Figure 3b. The result suggests two strong non−H-bonded interactions between −H of NH_4^+ and F of TF_2N, suggests the formation of a complex, and duly supports the proposed null hypothesis regarding the RTIL interaction with the ammonium ion. Also, we have visualized the theoretical output upon inclusion of the anion counterpart of the ammonium ion, which is nitrate, and the result is depicted in Figure 3c. The result suggests an increment of an interaction due to the presence of nitrate, along with existing interactions of the ammonium ion. The nitrate interaction has been captured between the N of NO_3^- and the N of imidazolium$^+$ ring, both possessing two different polarities, hence creating a nonbonded interaction.

We have also calculated the HOMO−LUMO energy gap for each individual entity to calculate the stability of the complex. The HOMO−LUMO computational visual output has been depicted in Figure 3d−f,[30] where Figure 3d represents the HOMO−LUMO orbital-mapped surface of the pristine RTIL, while Figure 3e represents the HOMO−LUMO output of the RTIL with NH_4^+ and Figure 3f represents the same for RTIL−NH_4NO_3. The computational visual output points out some unique features as most of the electron cloud has been observed to be situated at the bistriflimide group for both pristine RTIL and RTIL−NH_4^+ due to its strong negative polarity, which pulls the e^- cloud toward its vicinity. The e^- cloud, although observed to be shifted, hovers in between the $EMIM^+$-NO_3^- ring when introducing NO_3^-, probably due to the synergistic effect of NO_3^- pulling the e^- cloud toward its

https://doi.org/10.1021/acsomega.4c04181
ACS Omega 2024, 9, 33928−33934

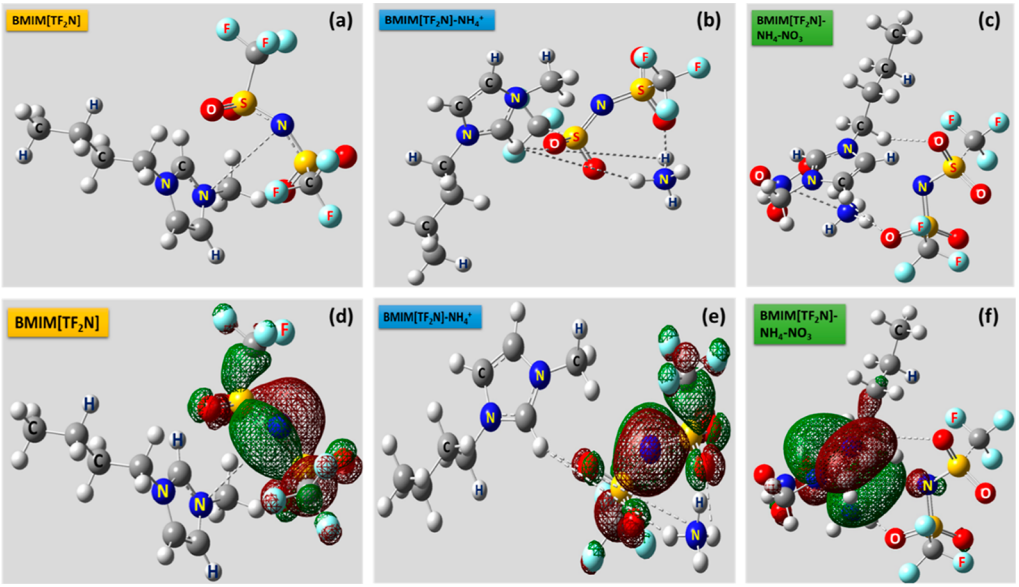

Figure 3. (a–c) Gaussian-optimized structure of (a) pristine RTIL: BMIM [TF_2N]; (b) interaction between BMIM [TF_2N] and the NH_4^+ ion; and (c) interaction between BMIM [TF_2N] and NH_4 NO_3 showing distinct noncovalent interactions including the −H-bonded interaction. (d–f) The HOMO−LUMO-mapped surface of (a–c) depicts unique e^- overlap, suggesting the formation of the complex.

vicinity. The result suggests that unique interactions make this transducing microenvironment rich with charges, which is helpful to build electrochemical sensors based on the principle of these interactions. The HOMO−LUMO energy gap of each interaction was calculated, and the result is presented in Table 2.

Table 2. Calculated HOMO−LUMO Energy of the RTIL, RTIL−NH_4^+, and RTIL−NH_4NO_3

compound	E_{HOMO} (hartree)	E_{LUMO} (hartree)
BMIM [TF_2N]	−0.38678	−0.03246
BMIM [TF_2N]$^-NH_4^+$	−0.49747	−0.12682
BMIM [TF_2N]$^-NH_4$ NO_3	−0.38564	+0.11274

The energy gap of RTIL−NH_4^+ and RTIL−NH_4NO_3 is calculated below

$$(E_{HOMO}^{BMIM[TF_2N]} - E_{LUMO}^{BMIM[TF_2N]-NH_4^+}) - (E_{LUMO}^{BMIM[TF_2N]} - E_{HOMO}^{BMIM[TF_2N]-NH_4^+})$$

$$= (-0.38678 - (-)0.12682) - ((-)0.03246 - (-)0.49747)$$

$$= (0.12682 - 0.38678) - (0.49747 - 0.03246)$$

$$= -0.25996 - 0.46501$$

$$= -0.72497 \text{ hartree}$$

$$(E_{HOMO}^{BMIM[TF_2N]} - E_{LUMO}^{BMIM[TF_2N]-NH_4NO_3}) - (E_{LUMO}^{BMIM[TF_2N]} - E_{HOMO}^{BMIM[TF_2N]-NH_4NO_3})$$

$$= (-0.38678 - 0.11274) - ((-)0.03246 - (-)0.38654)$$

$$= -0.49952 - 0.35318$$

$$= -0.8527 \text{ hartree}$$

It has been found that the HOMO−LUMO energy gap has been considerably reduced by 46% upon forming the complex with NH_4^+, whereas a staggering 54% reduction has been observed upon forming the complex with NH_4NO_3, which suggests the viability of the chosen interaction and hence supports the proposed null hypothesis.

We have also calculated the fundamental vibrational frequency of the pristine RTIL and the RTIL interaction with NH_4^+ in the absence and presence of NO_3^-. The result output as a function of absorbance has been depicted in Figures S1–S3, where Figure S1 represents the Fourier transform infrared (FTIR) absorption spectra of the pristine RTIL, whereas Figure S2 represents the RTIL interaction with NH_4^+ ions present. Figure S3 represents the absorption IR spectrum of the interaction between RTILs with both NH_4 and NO_3 ions present. All the major fundamental peaks are found to be observed and depicted in Table 3. The result suggests the presence of standard FTIR peaks, such as 838 cm^{-1} for the RTIL, which suggests the standard aromatic C−H stretching, corresponding to $BMIM^+$, whereas the peak at 1241 cm^{-1} depicts the standard C−F stretching of the TF_2N^- moiety. Important peaks observed for BMIM [TF_2N]$^-$ NH_4^+, such as

Table 3. Fundamental FTIR Peaks of Each Simulated Moiety

absorption peaks (cm^{-1})		
BMIM [TF_2N]	BMIM [TF_2N]$^-$ NH_4^+	BMIM [TF_2N]$^-$ NH_4NO_3
838 (aromatic C−H of $BMIM^+$)	581 (triflimide ring stretching)	1308 (−NO_2 stretching)
1052 (SO_2 stretching)	1094 (SO_2 stretching)	1390 (CF_3 of bistriflimide)
1142 (SO_2N of TF_2N^-)	1253 (tertiary C−H stretching)	1666 (BMIM−N−H stretching)
1241 (C−F stretching of TF_2N^-)	1499 (−NH_3 stretching)	2904 (N−CH_3 stretching)
2621 (BMIM−C−H stretching sym.)	2421 (−N−H stretching)	2978 (−NH−O stretching)

https://doi.org/10.1021/acsomega.4c04181
ACS Omega 2024, 9, 33928−33934

1499 cm^{-1}, suggest the presence of $-NH_3$ stretching, and the simulation result suggests the interaction of H of NH_4^+ with the N of $BMIM^+$, along with the peak at 2421 cm^{-1}, which depicts the individual stretching of NH_4^+. At the end, upon inclusion of NO_3^- in the system, new peaks appeared and were duly captured for BMIM $[TF_2N]^-$ NH_4NO_3 at 1308 cm^{-1}, suggesting the presence of $-NO_2$, and upon investigation, it has been found that the interaction is with the cation counterpart NH_4^+, whereas the whole compound is interacting with the RTIL individually. The FTIR result provides strong evidence regarding the interaction between the RTIL and the analyte ion, which ultimately lays the foundation to build the actual electrochemical sensor.

3.2. Sensor Calibration. The sensor response was calibrated against known spiked doses prepared as prescribed previously in Section 2 to cover the range from 0 to 32 ppm. As the PVC membrane contains ammonium ionophore I, ammonium ions have the highest probability of binding to the ionophore. This change in charge on the electrode surface can be measured using EIS. Figure 4a shows the decrease in the diameter of the semicircle in the Nyquist plot, which represents the charge transfer resistance R_{ct} in the Randles equivalent circuit. As the ammonium concentration in the soil increases, the impedance of the EDL decreases. The x-axis intercept of all measured signals is consistent, representing the electrolyte bulk resistance commonly termed R_s. The impedance at a 100 Hz frequency was used to build a linear regression model. Although a lower frequency would yield better sensitivity, environmental noise is dominant at lower frequencies. From the lab's previous work, frequencies below 50 Hz deviated significantly in situ compared to in-lab measurements. From the linear regression model, a spike and recovery plot with Pearson correlation for each soil type is presented in Figure 4b–d. All three soil textures had a Pearson $r > 0.991$, showing excellent accuracy of the sensor to quantify soil ammonium concentration.

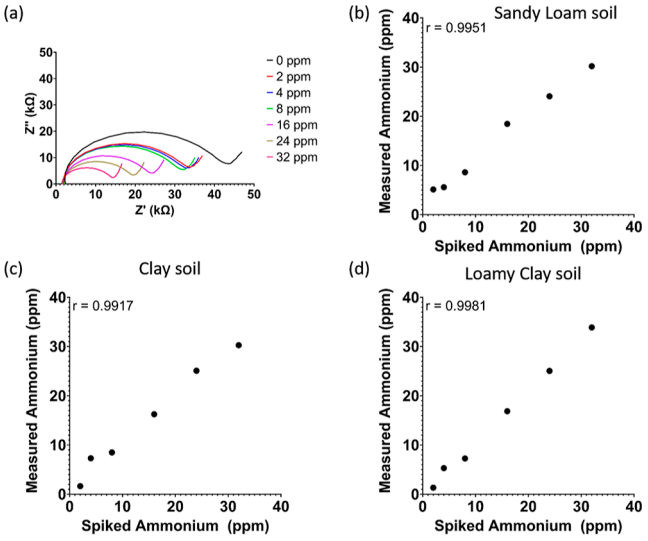

Figure 4. (a) Nyquist plot showing measured EIS in sandy loam soil of varying ammonium concentrations and (b) shows the measured vs spiked concentrations in sandy loam soil with a Pearson correlation $r = 0.9951$. For clay (c) and loamy clay soil (d), the Pearson $r = 0.9917$ and $r = 0.9981$, respectively.

3.3. Validation. To validate the accuracy of the sensor, five samples of varying soil textures from different agriculture farmlands around the world were acquired from our collaborator. The samples were analyzed using a spectrophotometer after ammonium extraction with a 1 M potassium chloride (KCl) solution. The ammonium concentration in the five samples was also measured by three different sensors. The measured averages, standard deviation, and calculated error percentage between the proposed sensor and reference method are reported in Table 4. The proposed sensor had a maximum error rate of 11% across all samples, indicating high accuracy. The coefficient of variance was below 13% across all samples, indicating good repeatability of the sensors.

Table 4. Sensor Validation Results

sample #	measured ammonium (ppm)	Std Dev	reference ammonium (ppm)	error rate (%)
S1-NH_4	5.56	0.56	5.12	8.59
S2-NH_4	16.71	1.76	15.43	8.30
S3-NH_4	3.89	0.34	3.68	5.71
S4-NH_4	32.67	3.99	29.58	10.45
S5-NH_4	48.19	4.89	44.22	8.98

3.4. In Situ Continuous Monitoring. A temporal study over 16 days was set up. Figure 5a demonstrates the study setup. A 19 L bucket was used to mimic an agriculture field. The soil used was from a grazing site in Overton, Texas, US, with an ammonium concentration of ∼4 ppm. A measurement was recorded once every 8 h for 16 days, as plotted in Figure 5b. It was observed that the sensor requires up to 24 h before stabilizing around the mean. Once a steady state is achieved, the measurements are within ±one standard deviation from the mean, indicating excellent reliability. Table 5 summarizes the mean, standard deviation, and coefficient of variation, excluding the first day. A coefficient of variance of 11%

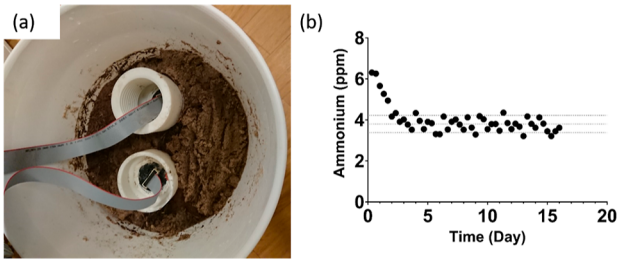

Figure 5. (a) Experimental setup showing the 19 L bucket filled to 1/3 with sandy loam soil with two sensor housings inserted. The ribbon cable connects to a laptop where a measurement is taken once every 8 h. (b) Measured ammonium concentration plotted against the number of days.

Table 5. Statistical Summary of the Temporal Study

number of values	45
minimum	3.2
maximum	5.3
range	2.1
mean	3.8
Std. deviation	0.42
Std. error of mean	0.062
coefficient of variation	11%

https://doi.org/10.1021/acsomega.4c04181
ACS Omega 2024, 9, 33928−33934

indicates high sensor stability even though the water content in the study was dynamically changing due to evaporation from the soil surface down to 15%. At this point, DI water was added to the soil, mimicking an irrigation cycle to maintain a moisture content between 15 and 60% throughout the study period. Although this occurred multiple times throughout the 16 days, the measured ammonium concentration stayed within one standard deviation from the mean indicated by the dotted horizontal lines. This proves that the measured signal is a direct representation of the ammonium concentration and is not driven by water content. The other takeaway from this temporal study is the rigidity of the EIS method against degradation of the reference electrode that occurs as the sensor sits in the soil for many weeks. When measuring open-circuit potential, the reference electrode's stability is of immense significance. As the reference electrode degrades over time, a drift is seen in the measured open-circuit potential.[18,25] Although the drift can be as minimal as 0.6 mV/day,[18] over the course of weeks, this shift becomes significant.

4. CONCLUSIONS

An ion-selective screen-printed electrode is presented for in situ soil ammonium sensing. The proposed sensor does not require any sample pretreatment, thus accurately measuring the ammonium concentration of unbuffered soil samples in the range of 2−32 ppm. EIS provides an ammonium-dependent response across the desired range, irrespective of the soil type. More importantly, EIS provides immunity at frequencies higher than 100 Hz against environmental noise that is dominant at lower frequencies. Three calibration curves were built to cover all soil types in the soil texture triangle. Sensor performance was validated against the gold standard spectrophotometer after potassium chloride extraction, which had a less than 20% error rate across the different soil types. A 16 day study also showed the stability of the sensor to measure ammonium concentrations over long periods with a coefficient of variance of 11%. This work presents a first-of-its-kind ammonium sensor for in situ continuous long-term monitoring.

■ ASSOCIATED CONTENT

Supporting Information

The Supporting Information is available free of charge at https://pubs.acs.org/doi/10.1021/acsomega.4c04181.

> Demonstrates the FTIR absorption spectra of pristine RTIL BMIM [TF2N], RTIL BMIM [TF2N] interaction with NH_4^+ ions, and RTIL BMIM [TF2N] interaction with NH_4 and NO_3 ions (PDF)

■ AUTHOR INFORMATION

Corresponding Author

Shalini Prasad − *Department of Bioengineering, University of Texas at Dallas, Richardson, Texas 75080, United States;* orcid.org/0000-0002-2404-3801; Phone: 972-883-4247; Email: shalini.prasad@utdallas.edu

Authors

Mohammed A Eldeeb − *Department of Bioengineering, University of Texas at Dallas, Richardson, Texas 75080, United States*

Vikram Narayanan Dhamu − *Department of Bioengineering, University of Texas at Dallas, Richardson, Texas 75080, United States*

Anirban Paul − *Department of Bioengineering, University of Texas at Dallas, Richardson, Texas 75080, United States*

Firas Maqsood Alam − *Department of Bioengineering, University of Texas at Dallas, Richardson, Texas 75080, United States*

E. Natalie Burgos − *Department of Bioengineering, University of Texas at Dallas, Richardson, Texas 75080, United States*

Sriram Muthukumar − *EnLiSense LLC, Allen, Texas 75013, United States;* orcid.org/0000-0002-8761-7278

Complete contact information is available at: https://pubs.acs.org/10.1021/acsomega.4c04181

Author Contributions

The manuscript was written through contributions of all authors. All authors have given approval to the final version of the manuscript.

Funding

The authors would like to thank and acknowledge the soil health data company Soil In Formation, PBC (SiF), for their role in funding this work. The funding source(s) played no role in the study design; in the collection, analysis, and interpretation of data; in the writing of the report; or in the decision to submit the report for publication.

Notes

The authors declare the following competing financial interest(s): Shalini Prasad and Sriram Muthukumar have a significant interest in Enlisense LLC, a company that may have a commercial interest in the results of this research and technology. The potential individual conflict of interest has been reviewed and managed by the University of Texas at Dallas and played no role in the study design; in the collection, analysis, and interpretation of data; in the writing of the report; or in the decision to submit the report for publication.

■ ACKNOWLEDGMENTS

The authors would like to acknowledge and thank Dr. Anil Somenahally (Texas A&M, AgriLife Extension, Overton) for his help in collecting and characterizing the sample using the soil science reference method.

■ REFERENCES

(1) United Nations. *SDG Indicators*, 2021; p 1095.

(2) *Food Security|Rising Food Insecurity*; World Bank, https://www.worldbank.org/en/topic/agriculture/brief/food-security-update (accessed 09 Apr, 2024).

(3) *Sustainable Agriculture Programs*; National Institute of Food and Agriculture, https://www.nifa.usda.gov/grants/programs/sustainable-agriculture-programs (accessed 19 May, 2023).

(4) Fan, Y.; Wang, X.; Funk, T.; Rashid, I.; Herman, B.; Bompoti, N.; Mahmud, M. S.; Chrysochoou, M.; Yang, M.; Vadas, T. M.; Lei, Y.; Li, B. A Critical Review for Real-Time Continuous Soil Monitoring: Advantages, Challenges, and Perspectives. *Environ. Sci. Technol.* **2022**, *56* (19), 13546−13564.

(5) Muangprathub, J.; Boonnam, N.; Kajornkasirat, S.; Lekbangpong, N.; Wanichsombat, A.; Nillaor, P. IoT and agriculture data analysis for smart farm. *Comput. Electron. Agric.* **2019**, *156*, 467−474.

(6) Deng, F.; Zuo, P.; Wen, K.; Wu, X. Novel soil environment monitoring system based on RFID sensor and LoRa. *Comput. Electron. Agric.* **2020**, *169*, 105169.

(7) Zhu, Y.; Chen, Y.; Ali, M. A.; Dong, L.; Wang, X.; Archontoulis, S. V.; Schnable, J. C.; Castellano, M. J. Continuous in situ soil nitrate sensors: The importance of high-resolution measurements across time and a comparison with salt extraction-based methods. *Soil Sci. Soc. Am. J.* **2021**, *85* (3), 677−690.
(8) Peng, X.; Chen, D.; Zhou, Z.; Zhang, Z.; Xu, C.; Zha, Q.; Wang, F.; Hu, X. Prediction of the Nitrogen, Phosphorus and Potassium Contents in Grape Leaves at Different Growth Stages Based on UAV Multispectral Remote Sensing. *Remote Sens.* **2022**, *14* (11), 2659.
(9) Kashyap, B.; Kumar, R. Sensing Methodologies in Agriculture for Soil Moisture and Nutrient Monitoring. *IEEE Access* **2021**, *9*, 14095−14121.
(10) Abenina, M. I. A.; Maja, J. M.; Cutulle, M.; Melgar, J. C.; Liu, H. Prediction of Potassium in Peach Leaves Using Hyperspectral Imaging and Multivariate Analysis. *AgriEngineering* **2022**, *4* (2), 400−413.
(11) Ullo, S. L.; Sinha, G. R. Advances in IoT and Smart Sensors for Remote Sensing and Agriculture Applications. *Remote Sens.* **2021**, *13* (13), 2585.
(12) Zedler, M.; Tse, S. W.; Ruiz-Gonzalez, A.; Haseloff, J.; Zedler, M.; Tse, W.; Ruiz-Gonzalez, A.; Haseloff, J. Paper-Based Multiplex Sensors for the Optical Detection of Plant Stress. *Micromachines* **2023**, *14* (2), 314.
(13) Potdar, R. P.; Shirolkar, M. M.; Verma, A. J.; More, P. S.; Kulkarni, A. Determination of soil nutrients (NPK) using optical methods: a mini review. *J. Plant Nutr.* **2021**, *44* (12), 1826−1839.
(14) Moraitis, M.; Vaiopoulos, K.; Balafoutis, A. T. Design and Implementation of an Urban Farming Robot. *Micromachines* **2022**, *13* (2), 250.
(15) Zhang, Z.; Zhang, X.; Rajh, T.; Guha, S. Photonic microresonator based sensor for selective nitrate ion detection. *Sens. Actuators, B* **2021**, *328*, 129027.
(16) Dudala, S.; Srikanth, S.; Dubey, S. K.; Javed, A.; Goel, S. Rapid Inkjet-Printed Miniaturized Interdigitated Electrodes for Electrochemical Sensing of Nitrite and Taste Stimuli,. *Micromachines* **2021**, *12* (9), 1037.
(17) Tian, H.; Gao, C.; Zhang, X.; Yu, C.; Xie, T. Smart Soil Water Sensor with Soil Impedance Detected via Edge Electromagnetic Field Induction. *Micromachines* **2022**, *13* (9), 1427.
(18) Joly, M.; Marlet, M.; Durieu, C.; Bene, C.; Launay, J.; Temple-Boyer, P. Study of chemical field effect transistors for the detection of ammonium and nitrate ions in liquid and soil phases. *Sens. Actuators, B* **2022**, *351*, 130949.
(19) Dai, C.; Song, P.; Wadhawan, J. D.; Fisher, A. C.; Lawrence, N. S. Screen Printed Alizarin-Based Carbon Electrodes: Monitoring pH in Unbuffered Media. *Electroanalysis* **2015**, *27* (4), 917−923.
(20) Dhamu, V. N.; Paul, A.; Muthukumar, S.; Prasad, S. DENSE: DiElectric Novel Soil Evaluation System to Electrochemically Profile Soil Matrices. *J. Electrochem. Soc.* **2022**, *169* (6), 067511.
(21) Zeitoun, R.; Biswas, A. Instant and Mobile Electrochemical Quantification of Inorganic Phosphorus in Soil Extracts. *J. Electrochem. Soc.* **2020**, *167* (16), 167512.
(22) Fayose, T.; Thomas, E.; Radu, T.; Dillingham, P.; Ullah, S.; Radu, A. Concurrent measurement of nitrate and ammonium in water and soil samples using ion-selective electrodes: Tackling sensitivity and precision issues. *Anal. Sci. Adv.* **2021**, *2* (5−6), 279−288.
(23) Garland, N. T.; McLamore, E. S.; Cavallaro, N. D.; Mendivelso-Perez, D.; Smith, E. A.; Jing, D.; Claussen, J. C. Flexible Laser-Induced Graphene for Nitrogen Sensing in Soil. *ACS Appl. Mater. Interfaces* **2018**, *10* (45), 39124−39133.
(24) Crespo, G. A. Recent Advances in Ion-selective membrane electrodes for in situ environmental water analysis. *Electrochim. Acta* **2017**, *245*, 1023−1034.
(25) Yupiter, R.; Arnon, S.; Yeshno, E.; Visoly-Fisher, I.; Dahan, O. Real-time detection of ammonium in soil pore water. *npj Clean Water* **2023**, *6* (1), 25.
(26) Gil, R. L.; Amorim, C. G.; Cuartero, M. Addressing the Detection of Ammonium Ion in Environmental Water Samples via Tandem Potentiometry-Ion Chromatography. *ACS Meas. Sci. Au* **2022**, *2* (3), 199−207.
(27) Eldeeb, M. A.; Dhamu, V. N.; Paul, A.; Muthukumar, S.; Prasad, S. Electrochemical Soil Nitrate Sensor for In Situ Real-Time Monitoring. *Micromachines* **2023**, *14* (7), 1314.
(28) Dhamu, V. N.; Paul, A.; Muthukumar, S.; Prasad, S. Electrochemical framework for dynamic tracking of Soil Organic Matter. *Biosens. Bioelectron.: X* **2024**, *17*, 100440.
(29) Dhamu, V. N.; Muthukumar, S.; Prasad, S. E-SCAN: Electrochemical Scanning of Carbonates, an In Situ Approach for Screening and Quantifying Inorganic Carbon in Soil. *J. Agric. Food Chem.* **2023**, *71*, 15954−15962.
(30) Dhamu, V. N.; Paul, A.; Muthukumar, S.; Prasad, S. Exploring the Role of Room Temperature Ionic Liquid as a Transducer in Electrochemical Soil Probing: A case study with [BMIM] [BF4]. *J. Electrochem. Soc.* **2021**, *168* (3), 037505.

https://doi.org/10.1021/acsomega.4c04181
ACS Omega 2024, 9, 33928−33934